Medially Based Meshing with Finite Element Analysis of Prostate Deformation

Jessica R. Crouch[1], Stephen M. Pizer[1], Edward L. Chaney[1], and Marco Zaider[2]

[1] Medical Image Display & Analysis Group
University of North Carolina at Chapel Hill
[2] Memorial Sloan-Kettering Cancer Center

Abstract. The finite element method (FEM) is well suited for use in the non-rigid registration of magnetic resonance spectroscopy images (MRSI) with intraoperative ultrasound images of the prostate because FEM provides a principled method for modeling the physical deformation that occurs when the MRSI intra-rectal imaging probe compresses and deforms the prostate. However, FEM requires significant labor and computational time to construct a finite element model and solve the resulting large system of equations. In particular, any finite element based registration method must address the questions of how to generate a mesh from an image and how to solve the system of finite element equations efficiently. This paper focuses on how m-rep image segmentations can be used to generate high quality multi-scale hexahedral meshes for use with FEM. Results are also provided that show m-rep geometry based point correspondences can be used to provide a good initial approximation to the solution of the finite element system of equations, thus reducing the required computation time. Results from the application of these methods to the registration CT images of a prostate phantom with implanted brachytherapy seeds are also presented.

1 Introduction

This paper considers finite element techniques for non-rigidly registering three-dimensional prostate images acquired for the purpose of brachytherapy planning and guidance. Brachytherapy involves implanting radioactive seeds in the prostate to treat prostate cancer. A magnetic resonance spectroscopy image (MRSI) can be used to design a seed placement pattern that targets suspected tumor deposits, but the process is complicated by the fact that the prostate appears compressed in the MRSI due to pressure from the intra-rectal imaging probe. Intra-operatively, the prostate is not deformed and seed placement is guided using ultrasound. Therefore, a non-rigid image registration is required to match points within the prostate shown in the MRSI planning image with the corresponding points in the intra-operative ultrasound image.

Other researchers have approached prostate imaging problems using methods that incorporate finite element analysis, in particular [4] and [8]. The work presented in [4] is most similar to the algorithm presented here, but differed from

ours in that it relied on manual segmentation and tetrahedral meshing, and a membrane model of the boundary rather than a solid object model was used in the computation of boundary conditions. The work presented in [8] employed a combined statistical and biomechanical approach.

The registration process used in this work consists of the following steps.

1. Fit a medial model, called an m-rep, to the prostate in both the undeformed and deformed images. The m-rep fit to the prostate in the undeformed image is referred to as the *model*, and the m-rep fit to the prostate in the deformed image is referred to as *model′*.
2. Build a multiscale finite element mesh from the *model*.
3. Derive boundary conditions that produce the observed shape change and minimize the energy of the deformation.
4. Assume the prostate is a linearly elastic body and compute its deformation using finite element analysis.
5. Apply the computed deformation to the undeformed image to register it with the deformed image.

Section 2 details how m-rep object models are used to automatically generate a mesh from an image. The method for determining boundary conditions from a pair of m-rep models is explained in section 3. The efficient solution algorithm is reviewed section 4. Results of this process applied to CT images of a prostate phantom are given in section 5, and future work is discussed in section 6. The meshing algorithm is explained most fully in this paper, while other aspects of the methodology are summarized. More algorithmic detail can be found in [5] for section headings marked with *.

2 Meshing Algorithm

The novel meshing algorithm presented here relies on m-rep object models to provide both global and local object shape information. An overview of m-rep models is presented, followed by an explanation of the meshing algorithm.

2.1 M-Rep Models

M-reps are medially based solid models that encapsulate more information about interior object shape than more traditional boundary based models. They also possess a number of characteristics that make them particularly well suited for modeling anatomic objects. For this application, the object based coordinate system provided by m-reps facilitates both the construction of the finite element mesh and the efficient solution of the finite element system of equations.

In the general case, an m-rep consists of a hierarchical tree of figures, where each figure represents a main component of an object or a protrusion or indentation of one of the main components. The simplest m-rep consists of a single figure which represents a slab-like region with a non-branching medial locus. Because the prostate's shape can be well represented with a single figure m-rep,

the discussion of m-reps here will be limited to single figure models. Readers are referred to [9]for a thorough explanation of m-reps, including multi-figure models.

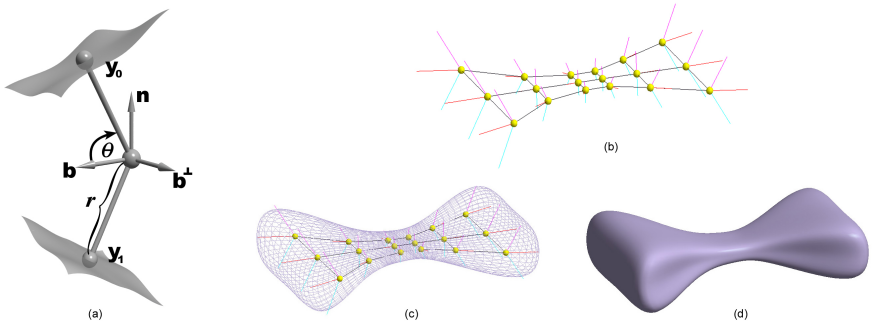

Fig. 1. (a) Diagram of a medial atom (b) A single figure m-rep model composed of a lattice of medial atoms (c) M-rep with wireframe object surface rendering (d) M-rep with solid object surface rendering

A figure is composed of a lattice of medial atoms. The structure of a single atom is illustrated in Fig. 1. Medial atoms are the smallest building blocks of an m-rep, and each stores the following information.

- x, position coordinates of the medial sheet at a sample point
- r, the radius, which is defined as the distance from x to the object boundary
- two vectors which originate at x and point to the boundary locations that an inscribed sphere at x with radius r would touch.
- θ, the angle between $\boldsymbol{b}$ and a boundary vector
- $F = (\boldsymbol{n}, \boldsymbol{b}, \boldsymbol{b}^{\perp})$, a frame that defines the tangent plane of the medial sheet at x and the direction $\boldsymbol{b}$ on the tangent plane that is in the ∇r direction

Atoms along the outer edges of the lattice have an additional variable, the elongation e. The elongation term allows control of the curvature around the crest of the object.

The lattice arrangement of medial atoms helps define an object based coordinate system for m-reps. Any point in an object can be referenced by its m-rep defined (u, v, t, τ) coordinates. The u and v directions coincide with the rows and columns of medial atoms in the lattice. τ ranges between 0 at the medial surface and ± 1 at the object surface, while t measures the angle between $+\theta$ and $-\theta$ in the crest region of the object. This object based coordinate system provides spatial and orientational correspondence between deformed versions of the same object. For example, in a prostate model a given set of (u, v, t, τ) coordinates will reference approximately the same part of the prostate using both compressed and uncompressed prostate m-rep models.

One advantage of the object based coordinate system is that a mesh defined using an m-rep's object based coordinates is automatically individualized to fit any deformed version of the m-rep model. This occurs because the mesh's object based coordinates do not change with deformation; only the mapping between object coordinates and world space changes when the m-rep is deformed. Another benefit of the object based coordinate system is the ability to express distances as a fraction of object width. This is convenient for mesh generation as it provides a natural way to size elements according to the proportions of an object.

In addition to the advantages offered by object based coordinates, m-reps are particularly attractive as part of an automatic meshing algorithm because they can be used to automatically segment objects from images [9]. In this work m-reps form a critical link between the image and the mesh generation process. Through the automatic segmentation procedure m-rep models are fit to image data, and then the geometry information stored in the m-rep is used to automatically generate a high quality finite element mesh.

2.2 Hexahedral Meshing Algorithm

Research has shown that for both linear elastic problems and non-linear elasto-plastic problems the error in a finite element solution is smaller for a mesh of linear hexahedral elements than for a mesh of similarly sized linear tetrahedral elements [3]. Current automatic meshing algorithms are much more successful at constructing quality tetrahedral meshes than quality hexahedral meshes, and the development of general purpose automatic hexahedral meshing algorithms is a problem that motivates current research efforts in the meshing community [11].

A quality hexahedral finite element mesh must have several characteristics.

- Compatibility – All interior nodes, edges, and faces must be shared by adjoining elements. This is a requirement for the finite element system of equations to converge monotonically [2].
- Good element shape – If the elements that compose a mesh are severely skewed, the convergence characteristics of the finite element system of equations is negatively impacted. If an element is inverted or the mesh folds, a valid finite element solution does not exist.
- Boundary fitted – The accuracy of the finite element solution is limited by how well the mesh represents the object's geometry. A mesh with elements that closely conform to the object boundary provides better representation of the geometry.

Some of the more promising hexahedral meshing algorithms developed have employed information about global object shape in the mesh design process. Price and Armstrong's work was based on decomposing an object into a set of geometric primitives using the medial axis [10]. More recently, the CUBIT team at Sandia has developed whisker weaving, an approach that uses a structure

called the spatial twist continuum (STC) to design a three dimensional hexahedral mesh that conforms to a given quadrilateral surface mesh for an object [6] [12].

The m-rep based meshing algorithm uses a standard meshing pattern for each figure of a model and assigns object based coordinates to each node. The mapping from object based coordinates to world space coordinates determines the nodes' placement in world space. A template based transition pattern is used to connect the mesh of a main figure with the mesh of a protrusion figure, but that part of the algorithm is not applicable to the single figure prostate problem.

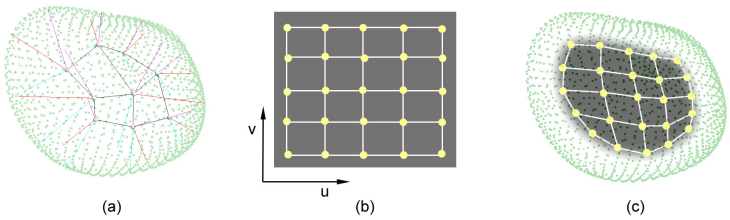

Fig. 2. (a) M-rep constructed from 3x3 lattice of medial atoms. (b) The (u,v) parameter plane of the medial surface with a 5x5 grid of sample points indicated. (c) Object with sample point interpolated and drawn on the medial surface.

The first step in meshing an m-rep figure is the construction of a sampling grid on the (u, v) parameter plane of the medial surface. The vertices of the sampling grid are placed at regular intervals in (u, v) coordinates, and their world space coordinates are calculated by interpolating a position on the medial surface. The spacing is determined by the ratio of the average thickness of the object to the average world space distance between medial atoms. Using this spacing, the average hexahedral element will have roughly equal dimensions. This process is illustrated in Fig. 2.

From the sampling grid on the medial surface, the coordinates of the other layers of nodes can be derived. For every (u, v) sample point except those around the outer rim of the medial lattice, five nodes are created at $\tau = -1, -.5, 0, .5, 1$. For sample points around the rim, a slightly different set of six nodes is created, with the sixth node sitting out on the object crest. The node and element patterns are illustrated in Fig. 3.

The basic four layer figure meshing pattern shown in Figs. 3, 4 and 5 provides a good coarse mesh of a figure and has the advantage of having no more than one face of any element lie on the surface of the object. This is important for the subdivision process described later. It also works well for objects with both high and low curvature crests.

Although the sample spacing is regular in medial coordinates, when the mesh is mapped into world space (x, y, z) coordinates the elements in narrower regions

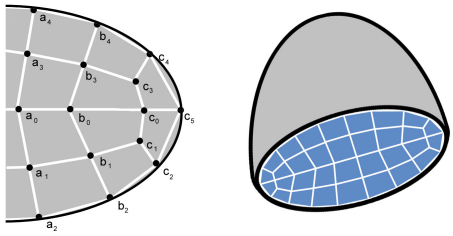

Fig. 3. Left: Three groups of nodes that are constructed from three corresponding medial surface samples. a_0 and b_0 are samples on the center portion of an object's medial surface that give rise to nodes a_0 - a_4 and b_0 - b_4, respectively. c_0 is a sample on the outer rim of the medial surface, from which nodes c_0 - c_5 are constructed.

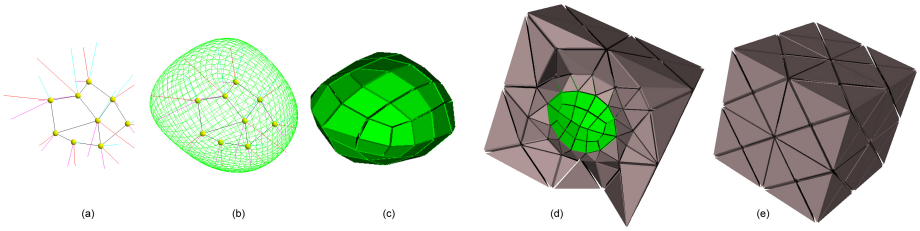

Fig. 4. (a) M-rep model of a prostate (b) Prostate m-rep with implied surface (c) Base level prostate mesh (d) Sliced view of the meshed volume of interest (e) Exterior view of the meshed volume of interest

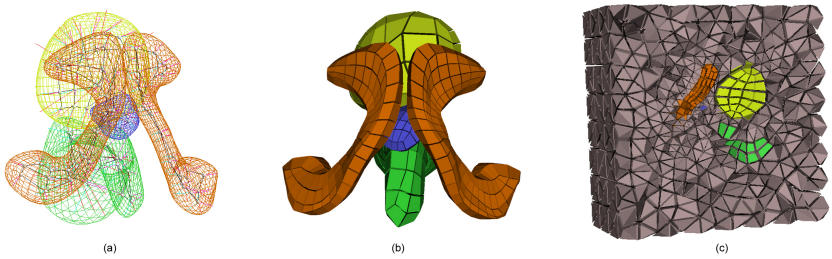

Fig. 5. (a) M-rep model of male pelvis, including pubic bones, rectum, bladder, and prostate (b) Mesh of male pelvis objects (c) Sliced view of object meshes with connecting pyramid and tetrahedral elements filled in

of the object tend to be smaller than the elements in wider areas. Typically, this is a desirable property, as a mesh usually needs to have smaller elements

in narrower parts of an object in order to sufficiently model the detail. This behavior flows naturally from the use of the m-rep object coordinate system.

Because the mesh construction is guided entirely by information contained in the m-rep model, the meshing process requires no user interaction.

2.3 Mesh Quality Optimization*

The shape quality of the majority of the elements generated by the m-rep based meshing algorithm is very good. However, elements generated near the corners of the parameterized medial surface or in areas of high curvature may have poorer shape. Therefore, after mesh construction the placement of some of the nodes is adjusted in an optimization of an element quality measure. In this process, nodes on the surface of an object have two degrees of freedom and are constrained to remain on the surface. Nodes in the interior of an object have three degrees of freedom. This optimization ensures that the mapping between the elements' parameter space and world space is well defined and does not fold.

2.4 Mesh Subdivision

If greater accuracy than provided by the initial coarse mesh is desired, then the initial mesh can be subdivided. The result is a mesh with smaller elements that provides a finer representation of the solution. The subdivision algorithm involves adding a node to the midpoint of each existing edge in the mesh, adding a node to the center of each existing quadrilateral face, and adding a node to the center of each existing hexahedral element. Fig. 6 shows the subdivision pattern for the three element types.

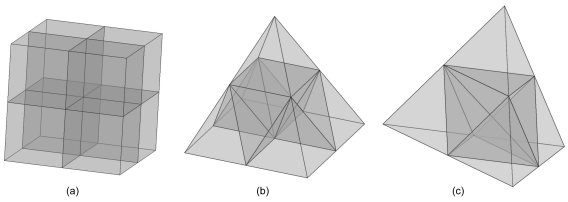

Fig. 6. Element subdivision patterns for (a) hexahedra (b) pyramid (c) tetrahedra

The hexahedral elements that represent the m-rep modeled objects have nodes with both world space (x, y, z) coordinates and medial (u, v, t, τ) coordinates. By subdividing these elements using their medial node coordinates, an improved, smoother approximation to the object geometry is achieved with subdivision. In contrast, straightforward subdivision with world space coordinates would also provide improved resolution for representing the solution but would

not reduce the geometric error or blockiness of the mesh. The medial coordinate based subdivision process allows for increased precision in both the geometry and the solution.

If adjacent faces of an element lay on the object surface, then the subdivision process described would lead to increasingly distorted and flattened elements since any surface patch is flat at a sufficiently small scale. The meshing pattern presented here has no elements with more than one face lying on the object surface, thus allowing good element shape to be maintained through an arbitrary number of mesh subdivisions.

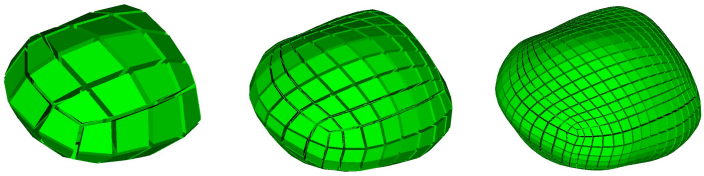

Fig. 7. A prostate mesh at three scale levels.

2.5 Meshing Space External to M-reps

In a multi-object deformation problem the space between the objects also needs to be meshed, and in a single object situation it is often useful to mesh space outside the modeled object. The m-rep meshing algorithm does not address this problem. Instead, a layer of pyramids is built on top of the quadrilaterals on the surface of the figure meshes. Then tetrahedra are built on top of the exposed triangular faces of the pyramids and used to mesh the remainder of the volume of interest.

The construction of the pyramids is straightforward. Each surface quadrilateral is taken as the base of a pyramid. The apex node is placed along the surface normal passing through the center of the quadrilateral base. The initial height of the pyramid is the average of the base edge lengths. When all the pyramids have been constructed, intersection tests are performed, and the height of any intersecting pyramid is reduced so that intersections are eliminated.

The construction of the tetrahedral mesh is performed using the tetrahedral meshing capability found in CUBIT [1]. Subdivision of the pyramid and tetrahedral elements outside the m-rep modeled object volumes is performed using the nodes' world space (x,y,z) coordinates. See Fig. 6 for an illustration of the subdivision patterns.

3 Boundary Conditions*

In order to compute a deformation with finite element analysis boundary conditions must be specified for some of the nodes either in terms of forces applied to the nodes or node displacements.

With an image registration problem, neither forces nor point displacements are available directly from the images. What is visible in the images is shifting and/or change in the shape of the boundary. M-reps provide a way to derive an initial approximation to point displacements from observed boundary changes in an image.

In the prostate case, the m-rep model that was fit to the original image and used to guide mesh construction is transferred onto the image of the deformed prostate and automatically fit to it. The original and deformed m-rep models have the same topology and their object based coordinates span exactly the same parameter space. This means that the m-rep's object based coordinate system defines a one to one geometry-based correspondence between points in the original and deformed prostate. This correspondence is used to define an initial set of displacement type boundary conditions.

In order to improve the accuracy of the computed deformation the boundary conditions are optimized. The ideal set of boundary conditions will produce a deformed version of the object such that

1. the surface of the deformed object matches the surface of the m-rep fit to the deformed image and
2. the physical energy needed to deform the object is minimized.

The assumption is that given two sets of boundary conditions that both result in the observed shape change, the one that requires the lesser amount of work is more likely.

The displacements are defined as the vectors that map points on the surface of $model$ to points on the surface of $model'$. In the optimization process the points on the surface of $model'$ are allowed to slide along its surface so that the displacements generated minimize the work of the deformation.

For the prostate phantom registration problem, the boundary condition optimization resulted in a 20% reduction in the energy of the deformation and an average change of .12 cm in the optimized boundary displacement vectors.

4 Solution Algorithm

4.1 Solution on the Initial Mesh

To compute a deformation, an NxN system of linear equation must be solved, where N is the number of nodes in the mesh. An initial approximation to the solution can be derived from the m-rep models by making use of the correspondence that exists between deformed versions of an m-rep. We estimate that the displacement of each node n_i is equal to the vector that maps $model(u_i, v_i, t_i, \tau_i)$ to $model'(u_i, v_i, t_i, \tau_i)$. A conjugate gradient algorithm is used to improve the approximate solution to within a set tolerance.

4.2 Solution on a Subdivided Mesh*

The system of equations that results from a subdivided mesh is much larger than the original system of equations, as seen in Table 1. The new larger system of equations can be efficiently solved by borrowing the idea from multigrid theory of solving the problem using meshes at different scales. The approach taken here is to solve the finite element system of equations on the initial mesh using the procedure outlined in Section 4.1, and then interpolate that solution to the subdivided mesh and solve again using the conjugate gradient solver. The number of iterations required to converge to a solution is reduced due to the good initial approximation provided by the solution on the coarser mesh. The interpolation - solution process may repeated as many times as desired to get an increasingly fine representation of the geometry and solution. The number of conjugate gradient iterations required to converge to the solution at the three subdivision levels is given Table 1. Note that the computational savings gained by starting with the m-rep predicted solution increases with the subdivision level.

Table 1. Solution Iterations Needed for Subdivided Mesh Levels

Subdivision Level	Nodes	Elements	Conj. Grad. Iterations with arbitrary initial approximation	Conj. Grad. Iterations with m-rep interpolated initial approximation
1	294	935	4	3
2	2,157	7,608	10	8
3	16,530	61,632	24	10

5 Registration Experiment

Because the clarity and resolution of CT images are superior to MRSI and ultrasound images, the initial validation study of the methodology was performed using CT prostate images. A male pelvis phantom was constructed at Memorial Sloan-Kettering Cancer Center, and CT images were acquired with an inflated and deflated MRSI probe in the phantom. The phantom prostate has seeds implanted in it, so the accuracy of the computed deformation can be examined by comparing the computed seed displacement with the observed seed displacement. For this test, the prostate m-rep model was used but the other pelvic structures were not explicitly modeled with m-reps. The area around the prostate was represented as a homogeneous region.

The linear elastic model has two elastic constants that characterize a material's stiffness: E, Young's modulus, and ν, Poisson's ratio. In this experiment the prostate was assigned $E = 60kPa$ and $\nu = .495$ based on the prostate tissue test results published in [7]. The meshed area exterior to the prostate was assigned $E = 10kPa$ and $\nu = .495$.

The locations of 75 seeds implanted in the phantom prostate were identified manually in both the uninflated and inflated CT images with .3 cm slice thickness. The computed deformation was applied to the seed locations in the uninflated image to predict the seed locations in the inflated image. The predicted seed locations were then compared to the observed locations in the inflated image. The average discrepancy between the predicted and observed locations was .27 cm, with a standard deviation of .14. The accuracy of the manual seed labelling was limited by the image slice thickness, and this limitation contributed to the error estimate. This is evident because when the within-slice error was examined separately from the across-slice error, it was found that the error components along the two high resolution image directions were on average .12 cm and .10 cm, while the average across-slice error was .25 cm.

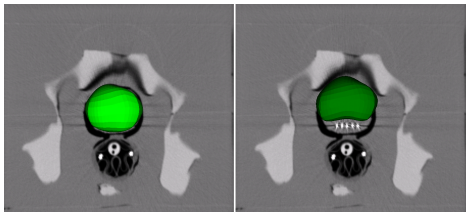

Fig. 8. Left: Original mesh of the prostate superimposed on a slice of the uninflated CT image. Right: Deformed mesh of the prostate superimposed on the same slice.

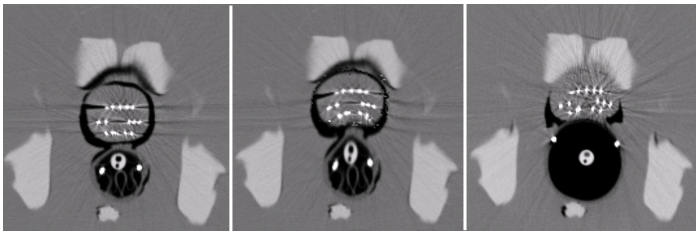

Fig. 9. Left: CT Slice of the phantom prostate with uninflated probe; Center: Slice after computed deformation has been applied; Right: Slice from CT of the phantom prostate with inflated probe

6 Future Work

The method is currently being tested using patient prostate images. Planned experiments also include the use of a five object male pelvis model that includes

the rectum, bladder, and pubic bone objects in addition to the prostate. The long term research plan is to apply this method to prostate images to improve brachytherapy planning and guidance.

7 Acknowledgements

This work was supported by NIH grant CA P01 47982 and by a Lucent GRPW fellowship. The authors would like to thank Gregg Tracton for assistance with image processing and Gilad Cohen for his prostate phantom design.

References

1. CUBIT information available at http://endo.sandia.gov/cubit/.
2. K Bathe. *Finite Element Procedures*. Prentice-Hall, New Jersey, 1996.
3. S E Benzley, E Perry, K Merkley, B Clark, and G Sjaardama. A comparison of all hexagonal and all tetrahedral finite element meshes for elastic and elasto-plastic analysis. *Proceedings, 4th International Meshing Roundtable*, pages 179–191, October 1995. www.andrew.cmu.edu/user/sowen/abstracts/Be172.html.
4. A Bharatha, M Hirose, N Hata, S Warfield, M Ferrant, K Zou, E Suarez-Santana, J Ruiz-Alzola, A D'Amico, R Cormack, R Kikinis, F Jolesz, and C Tempany. Evaluation of three-dimensional finite element-based deformable registration of pre-and intraoperative prostate imaging. *Medical Physics*, 28:2551–2560, Dec 2001.
5. J Crouch, S Pizer, E Chaney, and M Zaider. Medial techniques to automate finite element analysis of prostate deformation. *submitted to: IEEE Transactions on Medical Imaging*, Feb 2003. http://www.cs.und.edu/ jrc/TMI_JRC.pdf.
6. N T Folwell and S A Mitchell. Reliable whiskerweaving via curve contraction. *Proceedings, 7th International Meshing Roundtable*, pages 365–378, October 1998.
7. T A Krouskop, T M Wheeler, F Kallel, B S Garra, and T Hall. Elastic moduli of breast and prostate tissues under compression. *Ultrasonic Imaging*, 20:260–274, 1998.
8. A Mohamed, C Davatzikos, and R Taylor. A combined statistical and biomechanical model for estimation of intra-operative prostate deformation. *Proceedings, Fifth International Conference on Medical Image Computing and Computer-Assisted Intervention (MICCAI)*, pages 452–460, 2002.
9. S M Pizer, J Z Chen, P T Fletcher, Y Fridman, D S Fritsch, A G Gash, J M Glotzer, M R Jiroutek, S Joshi, C Lu, K E Muller, A Thall, G Tracton, P Yushkevich, and E L Chaney. Deformable m-reps for 3D medical image segmentation. *International Journal of Computer Vision*, submitted Sept. 2002. http://midag.cs.unc.edu/pubs/papers/IJCV01-Pizer-mreps.pdf.
10. M A Price and C G Armstrong. Hexahedral mesh generation by medial surface subdivision: Part II. solides with flat and concave edges. *International Journal for Numerical Methods in Engineering*, 40:111–136, 1997.
11. R Schneiders. Quadrilateral and hexahedral element meshes. In N P Weatherill J F Thompson, B K Soni, editor, *Handbook of Grid Generation*. CRC Press, Florida, 1998.
12. T J Tautges and S Mitchell. Progress report on the whisker weaving all-hexahedral meshing algorithm. *Proc. 5th International Conference on Numerical Grid Generation in Computational Fluid Simulations*, pages 659–670, 1996.